Available online at www.sciencedirect.com
ScienceDirect
Trans. Nonferrous Met. Soc. China 30(2020) 2861−2878
Transactions of Nonferrous Metals Society of China
www.tnmsc.cn

Effect of Cu addition on overaging behaviour, room and high temperature tensile and fatigue properties of A357 alloy

Lorella CESCHINI[1], Simone MESSIERI[2], Alessandro MORRI[1],
Salem SEIFEDDINE[3], Stefania TOSCHI[4], Mohammadreza ZAMANI[3]

1. Department of Industrial Engineering (DIN), Alma Mater Studiorum, University of Bologna, Viale Risorgimento 4, 40136 Bologna, Italy;
2. Ducati Motor Holding, Via Cavalieri Ducati Antonio 3, 40132 Bologna, Italy;
3. Department of Materials and Manufacturing, School of Engineering, Jönköping University, Gjuterigatan 5, 55111 Jönköping, Sweden;
4. Department of Civil, Chemical, Environmental and Materials Engineering (DICAM), Alma Mater Studiorum, University of Bologna, Viale Risorgimento 4, Bologna, Italy

Received 7 January 2020; accepted 16 July 2020

Abstract: The aims of the present work are to evaluate the overaging behaviour of the investigated Cu-enriched alloy and to assess its mechanical behaviour, in terms of the tensile and fatigue strength, at room temperature and at 200 °C, and to correlate the mechanical performance with its microstructure, in particular with the secondary dendrite arm spacing (SDAS). The mechanical tests carried out on the overaged alloy at 200 °C indicate that the addition of about 1.3 wt.% Cu to the A357 alloy enables to maintain ultimate tensile strength and yield strength values close to 210 and 200 MPa, respectively, and fatigue strength at about 100 MPa. Compared to the quaternary (Al−Si−Cu−Mg) alloy C355, the A357−Cu alloy has greater mechanical properties at room temperature and comparable mechanical behaviour in the overaged condition at 200 °C. The microstructural analyses highlight that SDAS affects the mechanical behaviour of the peak-aged A357−Cu alloy at room temperature, while its influence is negligible on the tensile and fatigue properties of the overaged alloy at 200 °C.

Key words: A357 alloy; C355 alloy; Al−Si−Cu−Mg casting alloy; tensile property; fatigue behaviour; high temperature; overaging

1 Introduction

Cast aluminium alloys are commonly employed to produce castings for automotive applications, in particular for engine parts, due to their high specific strength, excellent castability, and good corrosion resistance. Among the most important components, it is worth mentioning the engine block and the cylinder head. As reported by JAVIDANI and LAROUCHE [1], while in the past, such components were usually manufactured from cast iron because of its mechanical strength and high-temperature resistance, nowadays, the current increasing demand to limit fuel consumption and reduce pollutant emissions gradually has led designers to prefer lighter materials. In this sense, aluminium alloys possess lower density and high specific strength and are characterised by an excellent thermal conductivity, which allows the combustion heat to be extracted more rapidly compared to cast iron.

Among the most commonly employed alloys, ternary hypoeutectic alloys of Al−Si−Mg (e.g., A356 and A357 alloys) and Al−Si−Cu (e.g., A319) types should be mentioned. Al−Si−Mg and

Corresponding author: Alessandro MORRI; E-mail: alessandro.morri4@unibo.it
DOI: 10.1016/S1003-6326(20)65427-9

Al−Si−Cu alloys can be heat-treated to obtain elevated mechanical strength by precipitation hardening. According to JAVIDANI and LAROUCHE [1], peak-aged Al−Si−Mg alloys present good mechanical properties, elevated ductility and excellent castability; as a drawback, mechanical strength decreases with long-term exposure at high working temperatures (near or higher than 200 °C). Mg_2Si precipitates easily undergo diffusion-controlled coarsening leading to a progressive loss of their effectiveness in hindering dislocation slip, which results in loss of mechanical strength of the α(Al) matrix under the overaged conditions. Conversely, owing to the high content of Cu (3−4 wt.%), Al−Si−Cu alloys generally exhibit a higher mechanical strength and a superior overaging resistance in comparison to Al−Si−Mg, but are characterised by the lower ductility and castability, with a higher tendency to interdendritic shrinkages and hot tearing [1−3].

FARKOOSH and PEKGULERYUZ [3] pointed out that, in view of the specific conditions engine parts operate (which involve thermo-mechanical fatigue associated with the cyclic loading during engine heat-up and cool-down), a compromise between high tensile strength and ductility should be obtained to avoid undesired premature failure. Furthermore, the recent design trend has led to increase in the maximum engine working temperature and pressure, aiming to improve engine efficiency and to reduce fuel consumption and pollutant emissions by downsizing engines. As a result, the need for increased mechanical strength, superior thermal stability while maintaining good castability, led to the development of quaternary hypoeutectic Al−Si−Cu−Mg alloys, containing a limited content of Cu (≈1−2 wt.%), combining benefits of both Mg and Cu additions [4−10]. The simultaneous presence of Cu and Mg provided through aging treatment and the formation of *Q* quaternary precipitates ($Al_5Cu_2Mg_8Si_6$) characterised by higher coarsening resistance than the binary Al_2Cu or Mg_2Si have been reported by FARKOOSH and PEKGULERYUZ [3].

To design an alloy with a good compromise between high performance at the T6-state and overaging (related to the high Cu and Si levels), in which the hot tearing tendency induced by high Cu contents is minimised and good castability is maintained, is a challenge that needs to be addressed.

The aim of the present work was therefore to assess the microstructure and mechanical properties of a modified quaternary Al−Si−Cu−Mg alloy developed to produce motorbike engine heads. The alloy is designed based on a typical A357 alloy, containing 7 wt.% Si and 0.6 wt.% Mg, but with the addition of about 1.3 wt.% Cu. Compared to A354 and C355 quaternary alloys [8−10], employed at the industrial scale for cast engine parts, the A357−Cu alloy presents medium values of Si (compared to 9 wt.% and 5 wt.% for A354 and C355, respectively) and Cu (1.5 wt.% and 1 wt.% for A354 and C355, respectively) and slightly high values of Mg (0.5 wt.% for both A354 and C355). In particular, this study aims to: (1) evaluate the solutioning and hot isostatic pressing (HIP) temperatures, in order to avoid incipient melting; (2) assess the effect of secondary dendrite arm spacing (SDAS) on the mechanical strength; (3) evaluate the overaging behaviour of the alloy, by assessing its overaging curves and (4) investigate tensile and fatigue behaviours at room temperature and at 200 °C, both at the T6 condition and after overaging. A comparison with the most widely used Al−Si−Mg alloys (A356 and A357) and the high-performance Al−Si−Cu−Mg alloy (C355) with different SDAS values was also carried out, in order to assess the performance of the new alloy characterised by solidification-induced microstructural features similar to those of real sand and die castings.

2 Experimental

Castings of A357−Cu alloy were produced in a laboratory furnace according to the following experimental procedure. The molten base AlSi7Mg alloy was kept at 750 °C for about 3 h. An appropriate amount of Al−Cu and Al−Sr master alloys were added to reach the target composition (≈ 1.3 wt.% Cu, 150×10^{-6} Sr). Mg content was then properly tuned by the addition of Al−Mg master alloy. The melt was then poured into a permanent Cu die, pre-heated at 250 °C and with a graphite coating to avoid interaction between molten metal and mould. The chemical composition of the cast alloy was measured with an optical emission spectrometer (OES), and the results are listed in Table 1.

Table 1 Chemical compositions of A357−Cu casting and A356 and C355 alloys used for comparison, measured by OES (wt.%)

Alloy	Si	Cu	Mg	Fe	Mn	Ti	Sr	Al
A357−Cu	6.770	1.290	0.658	<0.03	<0.001	0.135	1.40×10^{-2}	Bal.
C355	4.990	1.050	0.470	0.138	0.021	0.133	2.10×10^{-2}	Bal.
A356	7.240	<0.001	0.420	0.138	0.007	0.120	1.50×10^{-2}	Bal.

The solidified cylindrical bars were then processed to obtain the desired secondary dendrite arm spacing (SDAS), by remelting the bars through a Bridgman furnace allowing controlled cooling conditions as described by SEIFEDDINE [11]. The bars were remelted at 730 °C for 30 min under Ar atmosphere, and then were directionally solidified by fixed machine speeds and cooling media (Table 2) to obtain cast samples characterized by fine (FS) and coarse (CS) microstructures, with average SDAS values ranging between 20−25 μm and 50−70 μm, respectively. Samples were then subjected to hot isostatic pressing (HIP) at 490 °C for about 2 h, in order to eliminate internal porosity, and were then heat-treated by solutionizing at 530 °C for 20 h, quenching in the water at 60 °C and artificially aged at 190 °C for 5.5 h. Table 3 shows the processing conditions of the tested alloy and those of the C355 and A356 alloys used for comparison.

Table 2 Bridgman furnace processing parameters and target SDAS values for samples with fine and coarse microstructures

Pulling velocity/(mm·s^{-1})	Cooling	Target SDAS/μm
0.3	Water	20−25 (FS)
0.03	Air	50−70 (CS)

Table 3 Heat treatment conditions of studied alloys

Alloy	HIP	Solution treatment
A357−Cu	490 °C, 2 h	530 °C, 20 h
C355	490 °C, 2 h	530 °C, 24 h
A356	490 °C, 2 h	535 °C, 4.5 h
Alloy	**Quenching**	**Aging at T6 condition**
A357−Cu	Water, 60 °C	190 °C, 5.5 h
C355	Water, 60 °C	180 °C, 6 h
A356	Water, 60 °C	160 °C, 4.5 h

Microstructural analyses were carried out on the as-cast and heat-treated samples, using optical microscopy (OM) and scanning electron microscopy equipped with energy-dispersive X-ray spectroscopy (SEM−EDS). Metallographic samples were cut from the as-cast and heat-treated samples, embedded in resin, then ground and polished by sandpapers and diamond suspensions up to 1 μm. Chemical etching with a 0.5% HF solution was then performed to highlighting microstructural features.

The secondary dendrite arm spacing was obtained by image analysis of the optical micrographs obtained for the as-cast alloy, calculated as the average on 15 images at 50-times magnification. The area fraction of intermetallic compounds was evaluated by contrast image analysis on SEM micrographs. In order to normalize the investigated area to the coarseness of microstructure, 14 fields at 500-times and 16 fields at 1500-times were analysed for coarse and fine samples, respectively, as described by CESCHINI et al [9].

Differential scanning calorimetry (DSC) analyses were carried out on as-cast and heat-treated samples, aiming to evaluate possible phase transformations occurring during heating. DSC was performed on 40 mg samples, under a purified argon atmosphere, employing a 10 °C/min scan rate in the temperature range of 25−680 °C.

The overaging behaviour of A357−Cu alloy was evaluated by subjecting T6-treated samples to high-temperature soaking at 200, 245 and 290 °C for fixed time intervals up to 168 h, then evaluating the corresponding hardness variation. Brinell hardness tests were carried out with 2.5 mm ball and 62.5 kg load, according to the ASTM E 10−18 standard [12] hereafter referred to as HB. The average of at least six measurements for each overaging condition was reported in the alloy overaging curves.

The tensile properties and fatigue behaviour of the A357−Cu alloy were evaluated in three different conditions: (1) at room temperature in the T6 condition (T6-RT), (2) at 200 °C in the T6 condition

(T6-200 °C) and (3) at 200 °C in the overaged condition induced by soaking at 210 °C for 41 h (OA-200 °C). The overaging temperature and time considered in the present study were chosen according to the typical average operating conditions of racing engine heads.

Round dog-bone tensile specimens (L_0=25 mm, gauge diameter d_0=5 mm) were machined from the heat-treated and overaged (subjected to soaking at 210 °C for 41 h) bars. Tensile tests were carried out at room temperature and at 200 °C on a screw-testing machine according to the ISO 6892-1 and ISO 6892-2 [13,14]. Tensile data were obtained from the data acquisition system and calculated as the average of at least three samples for each investigated condition. Samples tested at 200 °C were maintained at that temperature for 90 min aiming to homogenize the temperature before running the test.

Rotating bending fatigue tests were performed using the staircase method according to the UNI 3964 standard [15] to evaluate the 50% reliability endurance limit; fifteen samples for each investigated condition were tested. Fatigue samples were machined from the heat-treated and overaged (subjected to soaking at 210 °C for 41 h) bars; fatigue specimen sizes are shown in Fig. 1. Tests were carried out at 50 Hz of frequency, setting the run-out to 2×10^6 cycles. The A357−Cu alloy was tested both at room temperature and 200 °C, in the latter case allowing the temperature to homogenize before running the test for 60 min. The testing conditions are listed in Table 4.

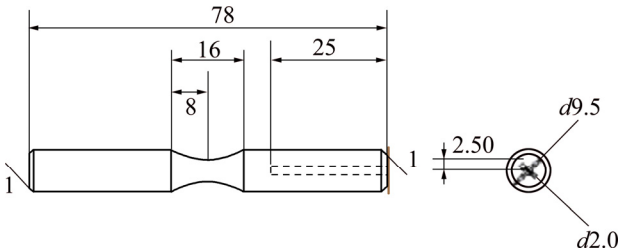

Fig. 1 Schematic diagram of fatigue sample (Unit: mm)

Fractographic analyses were carried out on both tensile and fatigue fracture surfaces by means of a multi-focus microscope and SEM−EDS, aiming to assess the mechanisms of failure and the crack nucleation sites.

A comparison of the overaging behaviour, the tensile and fatigue behaviour of the A357−Cu alloy with other (previously characterised [8,10,16]) ternary and quaternary Al-based alloys, namely the A356 (Al−Si−Mg) and C355 (Al−Si−Cu−Mg) alloys, was carried out.

Table 4 Tensile and rotating bending fatigue testing conditions (X=Performed, 0=Not performed)

Microstructural class	Heat treatment condition	Testing temperature	Tensile test	Fatigue test
Fine	T6	Room temperature	X	X
	T6	200 °C	X	0
	Overaged	200 °C	X	X
Coarse	T6	Room temperature	X	X
	T6	200 °C	X	0
	Overaged	200 °C	X	X

3 Results and discussion

3.1 As-cast microstructure

The microstructure of the as-cast A357−Cu alloy consists of primary α(Al) dendrites surrounded by the eutectic structure (Fig. 2). Due to the Sr modification, eutectic Si particles appeared evenly distributed and generally characterised by a fine fibrous morphology. However, differently from fine samples, coarse samples presented some areas with partially modified eutectic Si (Fig. 2(b)). This can be ascribed to the effect of the cooling rate on the modification of eutectic silicon particles, in agreement with previous works on different Al−Si alloys [8,9]. Results of SDAS calculations are listed in Table 5, highlighting a good agreement between the expected SDAS values and the measured ones.

3.2 Thermal analyses

Differential thermograms of as-cast and heat-treated A357−Cu samples are reported in Fig. 3. According to Refs. [17,18], Peaks 1−5 which were detected in the as-cast state of both FS and CS alloys, are consistent with the following reactions:

Peak 1: Formation of precipitates

Peak 2: Melting of Al_2Cu/Q-$Al_5Cu_2Mg_8Si_6$

Peak 3: Melting of Al−Si eutectic

Peak 4: Melting of α(Al)

Calculated areas and onset temperature corresponding to Peaks 1−4 are listed in Table 6 and are in agreement with data reported in elsewhere [17]. During heating, the alloy firstly

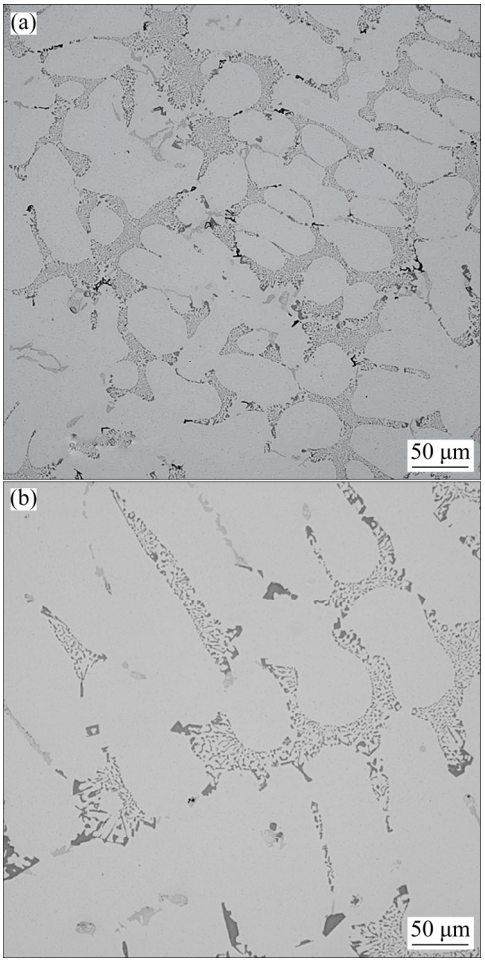

Fig. 2 Optical micrographs of as-cast A357−Cu alloy with fine (a) and coarse (b) microstructures

Table 5 Expected and measured SDAS values calculated on optical micrographs of FS and CS samples

Condition	SDAS/μm	
	FS	CS
Target	20−25	50−70
Measured	30±3	70±5

experiences the precipitation of intermetallic phases, at 240 °C. According to the literatures [3,19], this exothermic peak corresponds to the formation of quaternary Q-$Al_5Cu_2Mg_8Si_6$ precipitates. By increasing the temperature, before melting of the Al−Si eutectic and α(Al) (Peaks 3 and 4, respectively), an endothermic reaction (Peak 2) is observed, corresponding to the melting of Cu-bearing intermetallics (Q-$Al_5Cu_2Mg_8Si_6$ and θ-Al_2Cu) that developed during alloy solidification [7,20]. It has been reported that polynary eutectic phases (Q-$Al_5Cu_2Mg_8Si_6$) with a low melting point are formed when the Cu content is more than 2 wt.%, and the onset melting temperature is around 507 °C, while the melting point of Al_2Cu is around 520 °C.

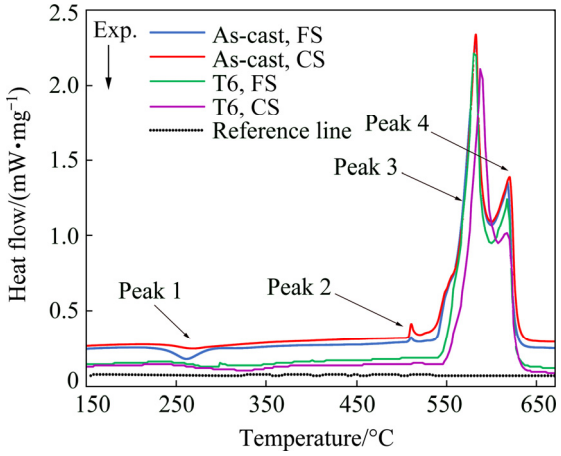

Fig. 3 DSC thermograms during heating of FS and CS samples

Table 6 Peak areas and onset temperature calculated on DSC thermograms of as-cast alloys

Peak	FS		CS	
	Heat/(J·g^{-1})	Onset temperature/°C	Heat/(J·g^{-1})	Onset temperature/°C
1	−13.07	235	−5.90	241
2	0.90	507	2.21	508
3	158.90	544	141.30	545
4	53.22	618	60.56	618

Such reaction is typical of quaternary alloys: the solution treatment temperature must be chosen according to this endothermic peak, to avoid the incipient melting and the generation of cavities within the casting. Solution treatment is therefore generally carried out: at a lower temperature, by optimisation of solution time, to fully homogenise and dissolve coarse solidification phases, or in multiple stages, the first at a temperature lower than that of the endothermic reaction (to dissolve the low melting compound) and the second at a higher temperature, to foster the alloying element's dissolution. In the latter case, if the alloy undergoes HIP, the HIP process replaces the first stage of the solution treatment; it is important, therefore, to carefully define the HIP temperature to dissolve coarse low-melting intermetallics and to avoid incipient melting.

By comparing the thermograms of FS and CS samples in the as-cast condition, two main

differences should be observed, related to Peaks 1 and 2, respectively. Peak 1, associated with the precipitation of *Q* phase, is more relevant in the FS sample compared to the CS sample. This difference, resulting in different peak areas (Table 6), is ascribed to the higher level of supersaturation induced by the higher solidification rate employed for the production of FS sample. It is therefore inferred that FS sample, in the as-cast condition, contains a lower amount of strengthening *Q* phase than the CS sample [3]; the *Q* phase, however, precipitates from the supersaturated solution during heating increasing the Peak 2 area. On the other hand, a coarse microstructure presents a more consistent Peak 2 in comparison to fine microstructure (2.214 vs 0.903 J/g), associated with the incipient melting of Cu-based phases. The lower solidification rate employed for CS sample, indeed, induced a higher level of segregation, thus a higher amount of low-melting compounds. After T6 treatment, it is observed that Peak 2 disappeared in both FS and CS samples. It is therefore inferred that Cu-based low melting compounds underwent complete dissolution, as a result of the solution treatment.

3.3 Evolution of microstructure with solution treatment

The evolution of microstructure with heat treatment was assessed by SEM analyses. In the as-cast state, Cu and Mg are entrapped in the coarse intermetallic particles formed during solidification. Their chemical composition, estimated by means of EDS analyses (Fig. 4), indicates that the stoichiometry of the observed particles is compatible with that of θ-Al_2Cu (both in eutectic and blocky morphology), Mg_2Si, π-$Al_8Mg_3FeSi_6$, Q-$Al_5Mg_8Cu_2Si_6$ [3,6,8−10]. Such intermetallics were observed both in FS and CS samples (Table 7), with a higher amount in the CS sample (about 1.60% area fraction) in comparison to the FS sample (about 1.40%). This result is in agreement with the previously reported DSC results (Fig. 2), showing higher energy associated with Peak 2 as a result of a higher segregation level induced by the lower solidification rate. Moreover, as previously observed in other quaternary alloys [8−10], the average size of intermetallic particles is strongly influenced by the solidification rate and, due to the higher time available for growth, the coarse microstructure is characterised by larger intermetallics in comparison to the fine one (Fig. 5). No β-Fe particles, were observed, either in fine or coarse microstructures, due to the low amount of Fe present in the alloy (~0.05 wt.%).

The evolution of coarse intermetallic particles with heat treatment, in terms of response to solutioning, was then assessed. As expected, the total area fraction of intermetallic particles decreases after T6 heat treatment. It should be noticed that the residual amount of intermetallics (Table 7) is lower for fine alloy compared to coarse microstructure (about 0.80% and 0.90% area fraction for FS and CS samples, respectively). This should be ascribed to the effect of microstructural fineness on the response to solution treatment. As previously observed, intermetallic particles contained in the FS sample are characterised by smaller size than those present in CS sample; as a result, diffusion mechanisms and, therefore, the dissolution of particles are facilitated.

With regard to the chemical composition of intermetallics after heat treatment, both in FS and CS samples, θ-Al_2Cu particles were dissolved to an acceptable degree, independently from their morphology (blocky or eutectic). It is known that eutectic and blocky particles are subjected to different dissolution mechanisms [7,20,21]: while the dissolution of eutectic Al_2Cu occurs by necking of the particle in several points, leading to subsequent fragmentation into small fragments and final dissolution, blocky phases undergo gradual dissolution of the entire particle, which generally requires longer time and higher temperatures. It is inferred that soaking the alloy at 530 °C for 20 h is sufficient to completely dissolve both the morphologies, regardless of size. Similarly, Mg_2Si particles are completely dissolved after T6 treatment. This is somehow expected since these particles are easily brought into solution by heat treatment, as reported by SJÖLANDER and SEIFEDDINE [20]. Differently, from Al_2Cu and Mg_2Si, quaternary phases such as π-$Al_8Mg_3FeSi_6$ and Q-$Al_5Mg_8Cu_2Si_6$ were still observed in the solution treated condition, independently from the microstructural fineness. *Q* and π phases are known to be stable also after long-term exposure to high solution treatment temperatures. It is possible that partial fragmentation occurred, but no quantitative analyses were carried out to check this.

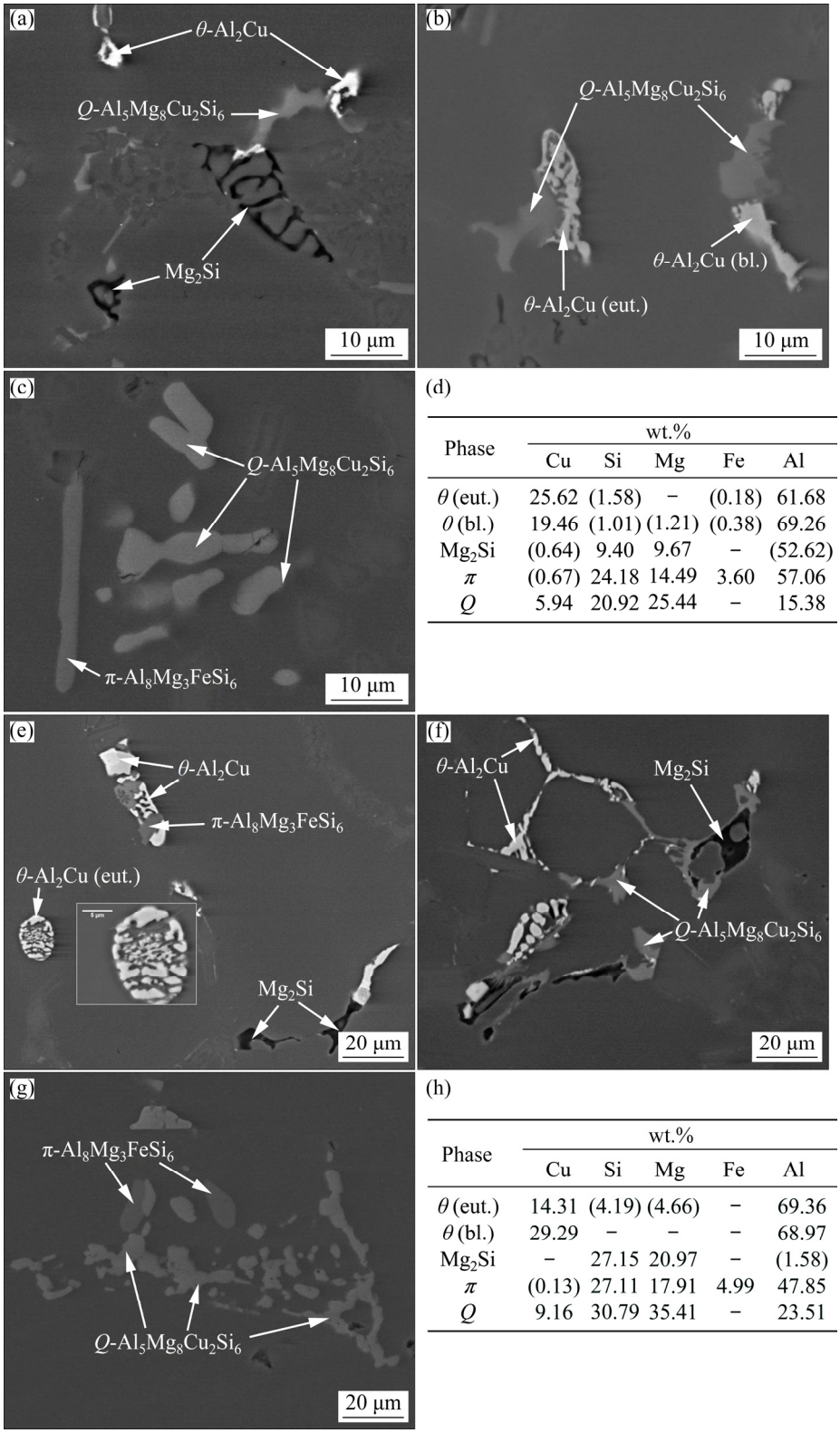

(d)

Phase	wt.%				
	Cu	Si	Mg	Fe	Al
θ (eut.)	25.62	(1.58)	−	(0.18)	61.68
θ (bl.)	19.46	(1.01)	(1.21)	(0.38)	69.26
Mg_2Si	(0.64)	9.40	9.67	−	(52.62)
π	(0.67)	24.18	14.49	3.60	57.06
Q	5.94	20.92	25.44	−	15.38

(h)

Phase	wt.%				
	Cu	Si	Mg	Fe	Al
θ (eut.)	14.31	(4.19)	(4.66)	−	69.36
θ (bl.)	29.29	−	−	−	68.97
Mg_2Si	−	27.15	20.97	−	(1.58)
π	(0.13)	27.11	17.91	4.99	47.85
Q	9.16	30.79	35.41	−	23.51

Fig. 4 SEM images and EDS analyses of intermetallics observed in FS (a−d) and CS (e−h) samples (The data in the brackets refer to elements present in the α(Al) matrix surrounding the analyzed phases)

3.4 Mechanical behaviour

3.4.1 Overaging effect on hardness

The effect of high-temperature exposure on the hardness of the A357−Cu alloy is shown in Fig. 6, which includes the overaging curves at 200, 245, and 290 °C for time up to 168 h. The starting condition is the T6 state, corresponding to a peak hardness value equal to HB 126. It is possible to

Table 7 Average intermetallic area fraction evaluated on FS and CS samples in as-cast state and after solution treatment

Sample	Average intermetallic area fraction/%	
	As-cast state	After solution treatment
FS	1.40	0.80
CS	1.60	0.90

observe that, in the first exposure time, increasing the overaging temperature from 200 to 290 °C leads to a more significant loss of hardness: after 4 h at 200 °C the hardness decrease is basically negligible (−2%), while at high temperatures of 245 and 290 °C loss of 21% and 45% with respect to the initial T6 condition is recorded. This behaviour can be ascribed to the diffusion-driven precipitates

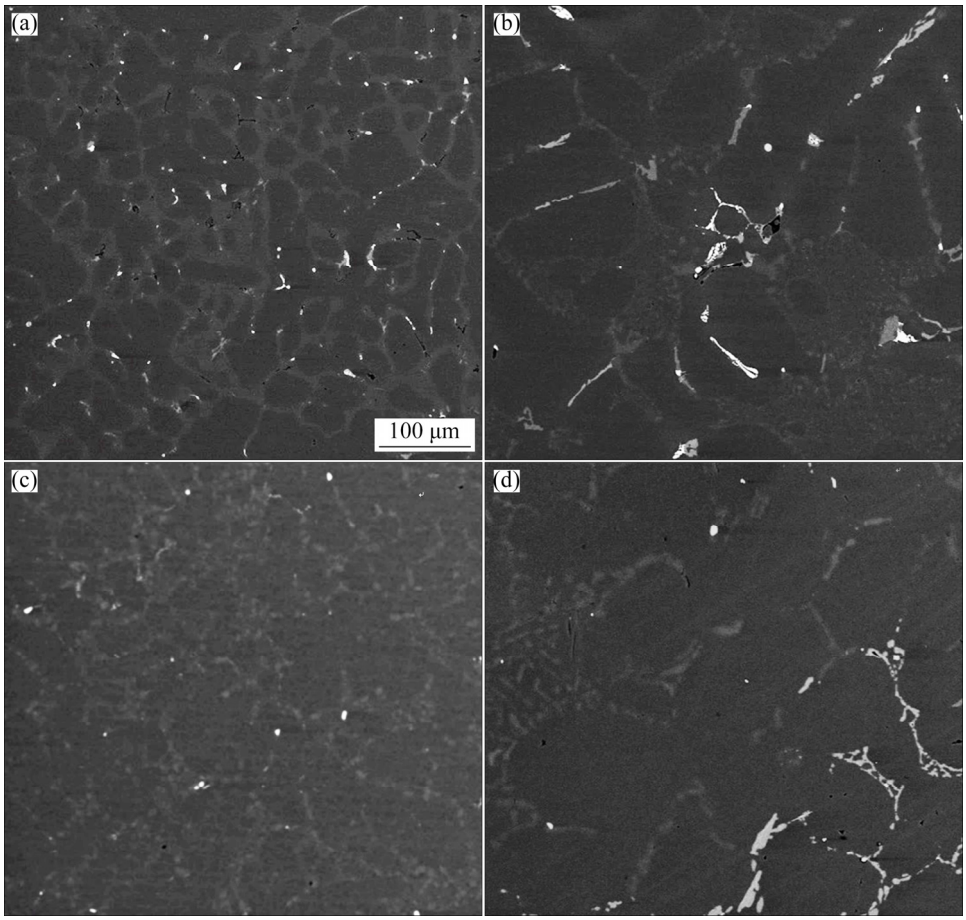

Fig. 5 SEM images of A357−Cu alloy in as-cast state for FS (a) and CS (b) samples and after T6 treatment for FS (c) and CS (d) samples

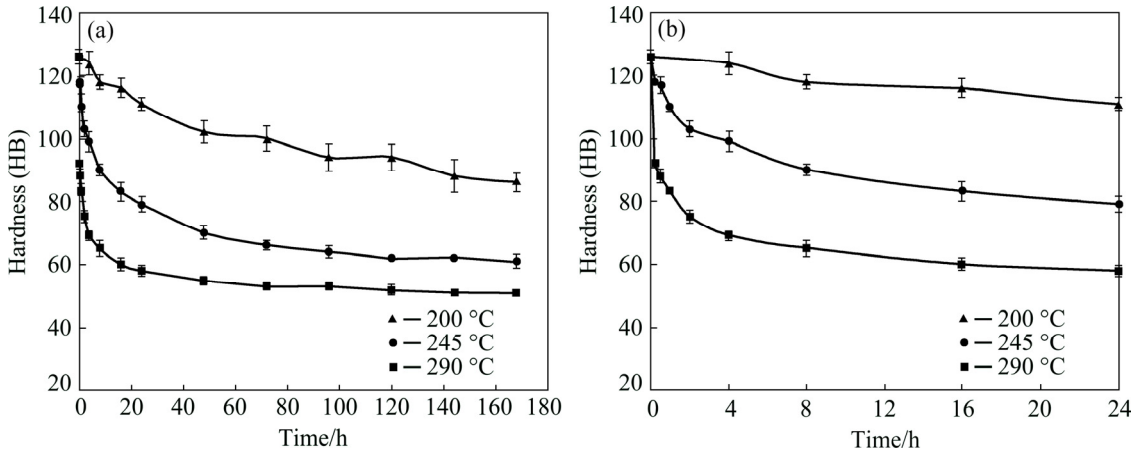

Fig. 6 Overaging curves of T6 A357−Cu alloy at 200 °C, 245 °C and 290 °C (a) and corresponding focus on the first 24 h (b)

coarsening phenomena occurring at high temperatures. While after 4 h at 200 °C no effect is obtained, by soaking at 245 and 290 °C, diffusion mechanisms are fostered. As a result, the strengthening precipitates formed by aging are subjected to a rapid coarsening, leading to a loss of coherence with the surrounding α(Al) matrix and the consequent decrease of alloy strength. Increasing the overaging time leads to a further decrease in hardness, depending on the soaking temperature. At 200 °C, and soaking time longer than 16 h, a gradual hardness decrease is recorded, reaching the minimum value of HB 86 for the maximum investigated time (168 h), corresponding to a 32% decrease compared to the starting condition. At 245 and 290 °C, growth and coarsening kinetics are so fast that most of the total hardness loss, compared to the T6 condition, occurs in the first 24 h. In this condition, the alloy lost 37% and 54% of its initial hardness at 245 and 290 °C, respectively. At these temperatures, hardness curves present a plateau, representing the minimum hardness values of HB 61 and HB 51 at 245 and 290 °C, respectively, corresponding to total decrease of 52% and 60% with respect to the starting condition.

A comparison of the overaging behaviour of the A357−Cu alloy with that of the A356 and A357 (Al−Si−Mg), and C355 (Al−Si−Cu−Mg) alloys is presented in Fig. 7 at temperatures of 200, 245 and 290 °C. The beneficial effect of adding Cu to A357 is clearly observable, leading to a significantly high residual hardness for the Cu-enriched alloy. Although the starting hardness is similar between the two alloys (HB 126 and HB 118 for A357−Cu and A357, respectively), the rate of hardness loss in the first 8 h is significantly higher for the A357 alloy. After about 48 h, a difference of about HB 20−30 is registered between the two alloys, remaining constant up to 168 h at all the tested overaging temperatures. Therefore, while the presence of Mg alone (generating Mg_2Si by precipitation hardening) makes A357 suitable for the production of components that work at temperature lower than 200 °C, the addition of Cu (enabling the precipitation of Cu-bearing phases and in particular of Q' as reported also by FARKOOSH and PEKGULERYUZ [3]), makes it possible to maintain high hardness values at 200 °C also for long soaking time (168 h).

The positive effect of Cu addition is even more evident at high temperatures. After 6 h of soaking at 245 °C and 290 °C, in fact, A357 alloy lost more than 50% of its initial hardness, while, at equal soaking time, the hardness losses of A357−Cu alloy are lower than 30% and 50% at 245 and 290 °C, respectively.

The graphs, moreover, indicate that the overaging curves at 200 °C of the A356 and C355 alloys are superimposed to those of A357 and A357−Cu alloy, respectively, while at 245 and 290 °C, C355 and A357 alloys have slightly higher hardness compared to A357−Cu and A356, respectively.

3.4.2 Tensile and fatigue tests

Results of mechanical tests carried out on the A357−Cu alloy are summarised in Fig. 8, where data of fine (SDAS 30 μm) and coarse (SDAS 70 μm) microstructures are compared. The T6 heat-treated alloy was tested both at room temperature and high temperature (200 °C), while the overaged alloy (after soaking at 210 °C for 41 h) only at high temperature.

The results of room temperature tensile characterisation confirmed the well-known beneficial effect of decreasing SDAS on tensile properties, as reported for other alloys [8,9]. The FS samples show higher yield strength (YS), ultimate tensile strength (UTS), elongation to failure (El), (≈5%, 8% and 40% respectively), compared to the CS ones. The intimate connection among UTS, El and SDAS has been documented in ternary Al−Si−Mg [22−25] and Al−Si−Cu systems [8,9]. The increase in YS, instead, is mainly related to the strengthening precipitates generated through precipitation hardening. The higher effectiveness of the solution treatment on smaller intermetallics present in FS, compared to larger intermetallics of the CS, may have lead to a higher degree of oversaturation [20,21] and consequently to the precipitation of a higher amount of strengthening precipitates during artificial aging. This is in agreement with microstructural observations, which shows a total area fraction of intermetallic particles after T6 heat treatment lower for the FS sample (≈0.8%) compared to the CS sample (≈0.9%). As previously observed, in fact, intermetallic particles contained in the CS alloy are characterised by a larger size than those present in FS samples. Their dissolution during solutioning, therefore, is more

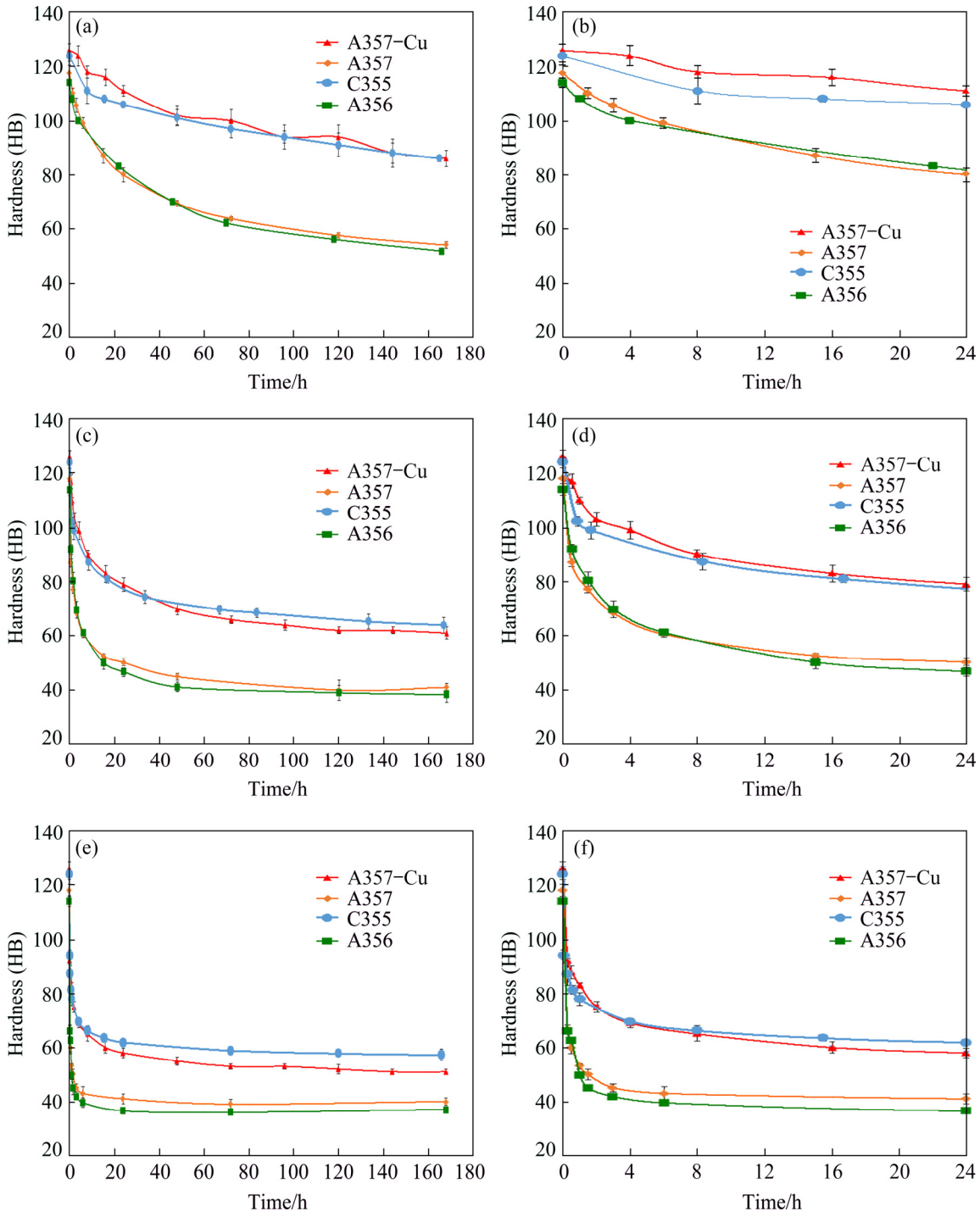

Fig. 7 Overaging curves of A357−Cu, A357, C355 and A356 alloys, and corresponding focus on the first 24 h of thermal exposure at 200 °C (a, b), 245 °C (c, d) and 290 °C (e, f)

difficult, and a higher amount of undissolved intermetallics is present in the CS alloy.

However, such difference in the mechanical behaviour between coarse and fine microstructures, is significant only in the T6-RT condition. At elevated temperature, indeed, the difference of tensile strength between CS and FS samples is strongly reduced, becoming almost negligible in the overaged state. At elevated temperatures, the common mechanisms which dominate the fracture process are softening of the α(Al) matrix (due to loss of coherency of the strengthening precipitates, which induces a decrease of both UTS and YS), and an increase of elongation to failure, independently

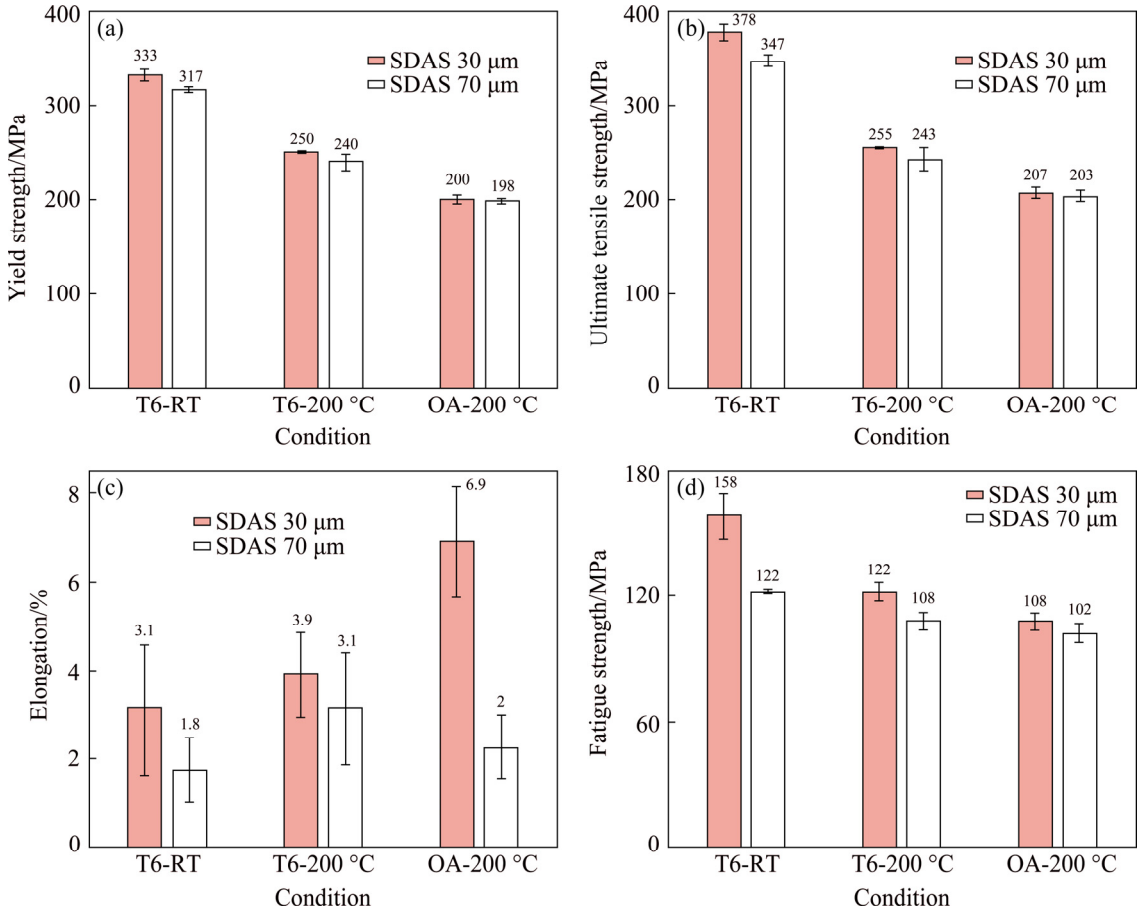

Fig. 8 Tensile properties and fatigue strength of A357−Cu alloy in three investigated conditions of T6 at room temperature (T6-RT), T6 at 200 °C (T6-200 °C) and overaged (soaked at 210 °C for 41 h) at 200 °C (OA-200 °C): (a) Yield strength; (b) Ultimate tensile strength; (c) Elongation to failure; (d) Fatigue strength at 2×10^6 cycles

from microstructural coarseness. The T6-200 °C samples displayed a reduction of 25%−30% of YS (from 333 to 250 MPa for FS, and from 317 to 240 MPa for CS) and UTS (from 378 to 255 MPa for FS, and from 347 to 243 for CS) and an increase up to 50% of elongation% (from 3.1% to 3.9% for FS and from 1.8% to 3.1% for CS) compared to the T6-RT samples. A further strength decrease was assessed in the overaged condition at 200 °C, consisting in a reduction of about 20% for both YS and UTS compared to the T6 condition at 200 °C (YS 200 MPa and 198 MPa, UTS 207 MPa and 203 MPa, for FS and CS, respectively). Overaging induces the coarsening of the strengthening precipitates, which lose their efficiency in hindering dislocation motion and facilitating plastic flow. The expected higher elongation of OA-200 °C compared to T6-200 °C samples was instead observed only for FS. This result was probably due to the presence of some large oxide inclusions observed in CS samples (see Section 3.5), which affected the elongation to failure, also increasing the data scatter.

With regard to fatigue behaviour (Fig. 8(d)), it is important to notice that the variation of fatigue strength, in all the investigated conditions, is well related to the results of tensile properties, in particular UTS. The correlation between UTS and the fatigue resistance has been observed by different studies on low and medium strength metallic materials [26−30], reporting the follow linear relationship:

$$\sigma_f = C\sigma_b \quad (1)$$

where σ_f is the fatigue strength (MPa), σ_b is the ultimate tensile strength (MPa) and C is a dimensionless coefficient that depends upon deformation and failure mechanisms that take place during fatigue [27,28].

Being the UTS and σ_f of the Al−Si alloys similarly affected by several microstructural features such as SDAS, eutectic Si particles, shape

and size of the intermetallic compounds, and the casting defects [23,24,31−34], UTS is generally considered the most appropriate static property to predict the fatigue behaviour of aluminium alloys. At equal heat treatment condition (T6), the fatigue strength of the investigated A357−Cu alloy decreases from room temperature to high temperature, and a further reduction is recorded in the overaged condition at 200 °C. Moreover, in agreement with the tensile results, the fatigue tests carried out at room temperature confirmed the beneficial effect of decreasing SDAS, as reported for other quaternary alloys by CESCHINI et al [10].

However, such a difference between the fatigue behaviour of coarse and fine microstructures is significant only in the T6-RT condition, as also previously mentioned for tensile strength (Figs. 8(a, b)). At elevated temperatures, the difference between fatigue strength of FS and CS decreases becoming substantially negligible in the overaged state. The elevated testing temperature, in fact, affecting the softening of the matrix independently from microstructural fineness, reduces the detrimental effect of coarse phases (eutectic silicon, intermetallics) and casting defects (oxides), which could promote crack nucleation during cyclic loading. Therefore, CS samples, which have a higher volume fraction of quaternary phases (0.90% and 0.80% for CS and FS respectively) and a higher amount of oxides (see Section 3.5) compared to FS samples, can benefit more from temperature increase compared to FS, by relaxation of the stresses at the interface between matrix and intermetallic particles or inclusions. The results of fatigue tests, indeed, point out that the reduction of fatigue strength induced by testing temperature and overaging condition is always higher for FS compared to CS: from T6-RT to T6-200 °C, σ_f reductions of 23% and 11% were measured for fine and coarse microstructures, respectively. Similarly, from T6-RT to overaged-200 °C, the measured decrease was 30% for FS but only 16% for the CS (Table 8).

The beneficial effect of the enhanced plasticity of the matrix on the fatigue behaviour of the alloy at high temperature is also supported by the trend of the σ_f/σ_b ratio of C, which increases moving from T6-RT to the OA-200 °C condition (Table 8), confirming that fatigue strength is less affected by increasing temperature than σ_b. Moreover, since the coefficient C depends upon failure mechanisms that take place during fatigue [27,28], it can be supposed that SDAS has no appreciable effect on the failure mechanisms at high temperature, but it could induce slightly different failure mechanisms in the alloy at room temperature, due to the different volume fraction and size of intermetallic and/or the presence of oxides, as can be inferred by the difference in the coefficient C between FS and CS.

In view of these results, it is possible to say that the effect of SDAS on mechanical behaviour at 200 °C is strongly reduced in A357−Cu castings for high-temperature applications in the case of long-term thermal exposure leading to overaging phenomena. In these conditions, differently from room temperature in the T6 condition, a fine microstructure is not significantly beneficial in terms of UTS, YS, and σ_f.

Based on previous investigations [8−10,16], the tensile and fatigue properties of A357−Cu alloy were compared with those of a ternary Al−Si−Mg alloy (A356) and a quaternary Al−Si−Cu−Mg alloy (C355) with similar SDAS values (≈25−30 μm). Data, summarised in Fig. 9, should be interpreted in the light of the overaging curves reported in Fig. 7, representing the capability of the alloys to withstand long-term high- temperature soaking. It is possible to observe that, in general, quaternary alloys present superior mechanical strength both at room and high temperatures than the ternary ones. This should be ascribed to the presence of both Cu and Mg, leading to the formation of θ (Al_2Cu) and Q ($Al_5Cu_2Mg_8Si_6$) in addition to

Table 8 Fatigue strength at 2×10^6 cycles (σ_f), ultimate tensile strength (σ_b), ratio of σ_f to σ_b (C), for FS and CS samples

Condition	FS			CS		
	σ_f/MPa	σ_b/MPa	C	σ_f/MPa	σ_b/MPa	C
T6-RT	158±11	378±9	0.42	122±3	347±5	0.35
T6-200 °C	122±4	255±1	0.48	108±4	243±12	0.44
OA-200 °C	108±4	207±6	0.52	102±4	203±6	0.5

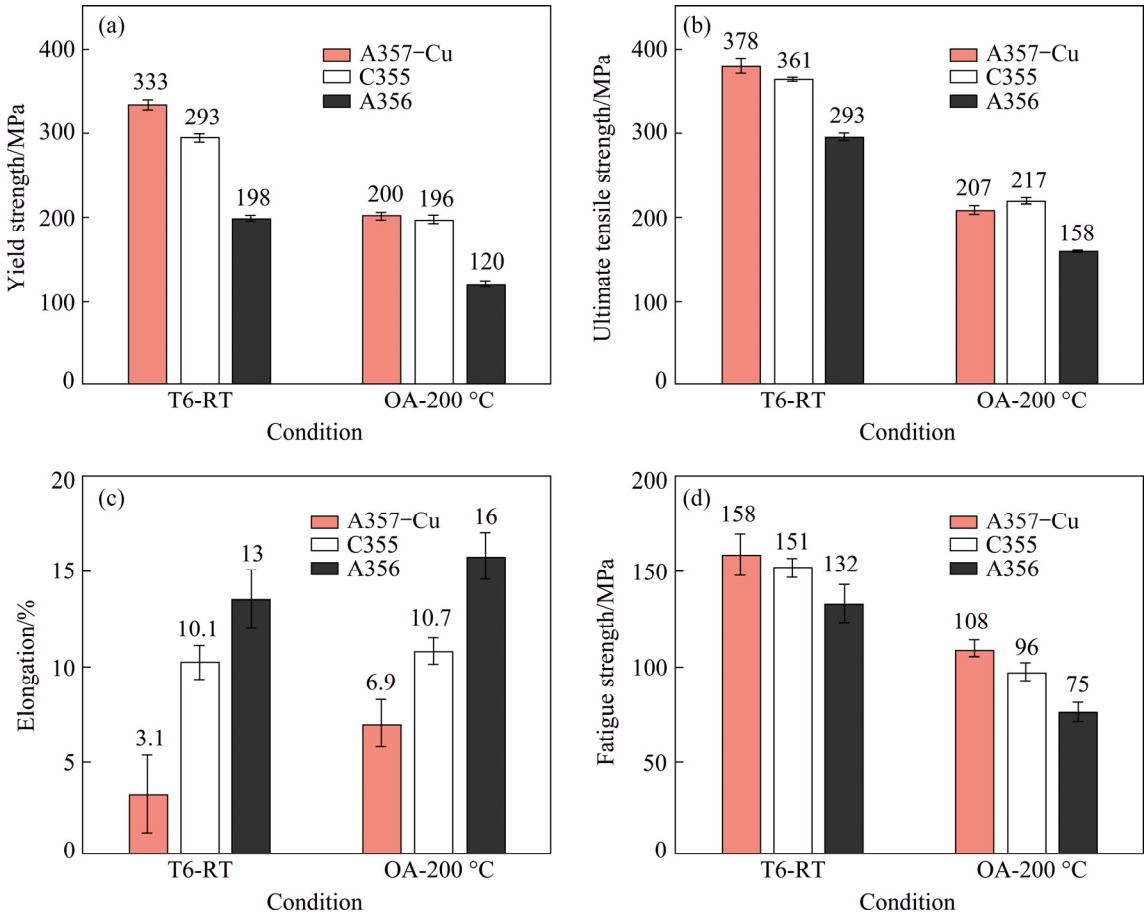

Fig. 9 Comparison of tensile properties and fatigue strength of A357−Cu, C355 and A356 alloys at similar SDAS values (25−30 μm): (a) Yield strength; (b) Ultimate tensile strength; (c) Elongation to failure; (d) Fatigue strength at 2×10^6 cycles (Data of both FS (SDAS 30 μm) and CS (SDAS 70 μm) samples are compared)

Mg_2Si strengthening precipitates upon T6 heat treatment. As also inferred by overaging curves, ternary A356 is characterized by limited resistance to overaging, showing a remarkable loss of UTS, YS and σ_f in the overaged condition at 200 °C. The YS decreases from 198 to 120 MPa, the UTS decreases from 293 to 158 MPa and σ_f decreases from 132 to 75 MPa, considerably lower than the UTS decrease (≈210 MPa), the YS (≈200 MPa) and fatigue strength (≈100 MPa) of quaternary Al−Si−Cu−Mg alloys in the same condition.

By comparing the mechanical behaviour of the quaternary alloys A357−Cu and C355 alloys, instead, it is possible to point out that at room temperature A357−Cu T6 presents a YS that is higher by about 13% (333 vs 293 MPa) and UTS is higher by about 5% (378 vs 361 MPa) compared to C355. In the overaged condition at 200 °C, instead, the C355 T6 has similar YS (196 vs 200 MPa) and UTS (217 vs 207 MPa) compared to overaged A357−Cu. Moreover, the C355 alloy, both in T6 and overaged condition, shows better ductility compared to A357−Cu alloy.

A deep understanding of the different mechanical behaviours between the A357−Cu and C355 alloys may be provided only by means of TEM analyses of the strengthening precipitates. This activity was not the object of the present research, which was focused on the assessment of the mechanical performance of the alloy in relation to solidification microstructural features, such as SDAS, large intermetallics and defects. Nevertheless, a possible explanation for the mechanical behaviour of the alloy is proposed, based on a literature survey. The following aspects were evaluated: (1) different strengthening effects on tensile properties at room and high temperature performed by θ' and Q' phases; (2) influence of Cu and Mg content on the precipitation of hardening phases. With regard to the strengthening effect, θ' remarkably increases the hardness of the Al alloys at room temperature; Q', instead, has a lower

strengthening effect at room temperature but higher coarsening resistance and, therefore, superior effectiveness in strengthening the alloys at high temperature [3,35,36]. Consequently, the increased amount of θ' increases the performance of the alloy mainly at room temperature, while Q' leads to an improvement of the mechanical properties mainly at high temperature. With regard to the precipitation kinetic, in Al−Si−Cu−Mg alloys with high Cu and Mg content and high Cu/Mg ratio (both A357−Cu and C355 have a Cu/Mg mass ratio of about 2) the increase of Cu and Mg contents promotes the precipitation of the θ' compared to the Q' [35,37]. Since A357−Cu has higher content of both Cu and Mg compared to C355, it can be inferred that its higher performance at room temperature compared to C355 is probably due to its higher amount of θ' formed after aging compared to the C355. A similar amount of Q' can instead explain the slight difference of the tensile behaviour of the alloys at 200 °C in the overaged condition.

The higher level of θ' in the A357−Cu compared to C355 alloy, moreover, is the reason for the lower ductility of A357−Cu as reported by ZHENG et al [35].

The comparison of fatigue behaviour of the two alloys (Fig. 9) shows the higher performance of the A357−Cu alloy compared to C355 both in the T6 condition at room temperature and in the OA condition at 200 °C. While the result at room temperature is in agreement with the tensile test data, the higher fatigue resistance of the A357−Cu alloy at 200 °C can be explained taking also into account, among other things, the different amounts of intermetallic particles present in the two alloys, which can act as fatigue cracks nucleation sites. The average area fraction covered by intermetallics in the C355 alloy, investigated by CESCHINI et al [10], is about 1.2% compared to the 0.8% of the A357−Cu alloy. This difference is mainly due to the different contents of Fe in alloys (~0.140 wt.% and <0.03 wt.% for C355 and A357−Cu alloy, respectively), which induced the formation of a higher amount of Fe-rich phases, such as blocky π-Fe ($Al_8Mg_3FeSi_6$) and acicular β-Al5FeSi or Al−Cu−Fe, in C355 compared to A357−Cu. Moreover, while the presence of the detrimental acicular β-Al_5FeSi phase was clearly documented in the C355 alloy, no β phase was observed during microstructural or fractographic analyses in the A357−Cu alloy. The harmful role played by the intermetallic particles on the C355 fatigue strength was confirmed by the fact that in the C355 alloy the crack nucleation sites were mainly in correspondence of coarse Fe-rich phases as reported by CESCHINI et al [10], while in the A357−Cu alloy they were next to oxides (Fig. 10).

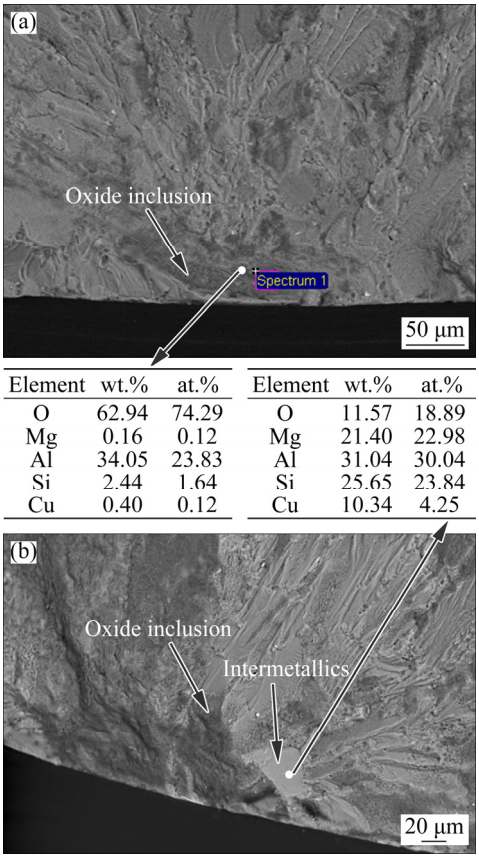

Element	wt.%	at.%
O	62.94	74.29
Mg	0.16	0.12
Al	34.05	23.83
Si	2.44	1.64
Cu	0.40	0.12

Element	wt.%	at.%
O	11.57	18.89
Mg	21.40	22.98
Al	31.04	30.04
Si	25.65	23.84
Cu	10.34	4.25

Fig. 10 SEM images and EDS analyses of crack nucleation sites of FS T6-RT fatigue specimen tested at 150 MPa and failed after 2.6×10^5 cycles where oxide inclusion is present (a) and CS OA-200 °C fatigue specimen tested at 100 MPa and failed after 7.95×10^5 cycles where both oxide inclusion and large intermetallics are visible (b)

Therefore, while for the A357−Cu alloy in the OA condition the softening of the matrix at 200 °C could balance the negative effect of small differences (~0.1%) of average area fraction covered by intermetallics between FS and CS samples, the high temperature could not completely compensate for: (1) the higher area fraction of intermetallics (~0.4%) present in the C355 compared to A357−Cu; (2) the presence of the detrimental phase in the C355, not observed in the A357−Cu alloy.

3.5 Fracture surfaces

Low magnification multi-focus images of the fracture surfaces of tensile specimens are shown in Fig. 11. These highlight the presence of large oxide inclusions (black zones on the surface), mainly in samples with coarse microstructure, probably due to incomplete removal of suspended oxides from the liquid metal before the pouring process. The presence of such defects is considered to be the main reason for the recorded scatter in elongation of the alloy (Section 3.4.2). Samples with large oxides, indeed, have a very low elongation; in the range of 30% and 40% of the average elongation, irrespective of heat treatment and test conditions. SEM images at high magnification of the tensile fracture surfaces (Fig. 12) reveal the presence of ductile fracture morphology typical of Al−Si−Mg−Cu casting alloys. The failure mechanisms consist of decohesion and/or cracking of brittle eutectic Si and intermetallic particles, generation of shear bands with consequent formation of microcracks and the final fracture generated by linkage of microcracks and their propagation [8,9,24,38,39]. However, while FS samples present fine and homogeneously distributed dimples on the fracture surface, CS samples are characterised by larger dimples and a more pronounced interdendritic fracture path, due to the presence in these regions of large Cu-rich intermetallics, which crack during the tensile test (Fig. 13). The slightly different fracture mechanisms between FS and CS samples, and the presence of larger oxide inclusions, justify the lower elongation to failure of the latter (Fig. 8). Except for a more pronounced ductile morphology no substantial differences were observed between the fracture surfaces of samples tested at room temperature or 200 °C.

Fracture surface analyses of fatigue samples highlighted that in almost all the tested specimens (independently from SDAS and test condition), fatigue cracks nucleated in the outer zone of the specimen, right by large oxides or small oxides close to intermetallic particles (Fig. 10). This

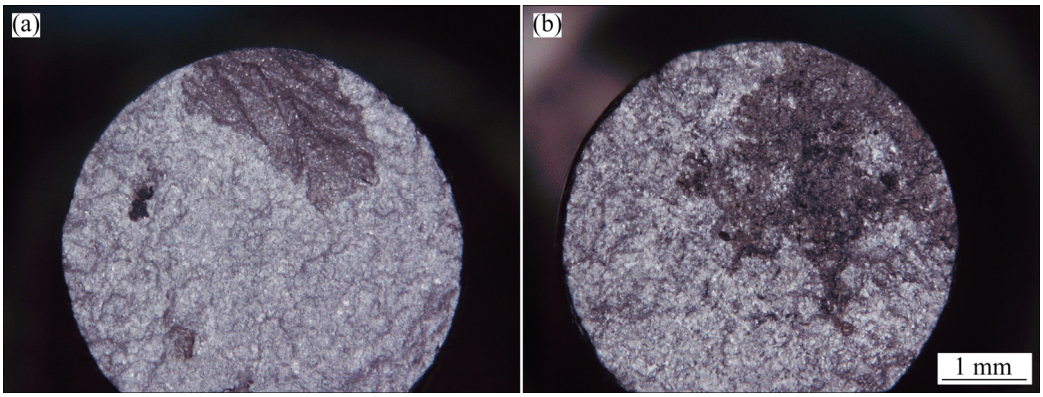

Fig. 11 Multifocus images showing presence of large oxide inclusions (black zones) on fracture surfaces of FS T6-RT sample (a) (YS=335 MPa, UTS=353 MPa, Elongation=1.2%) and CS OA-200 sample (b) (YS=195 MPa, UTS=196 MPa and Elongation=0.8%)

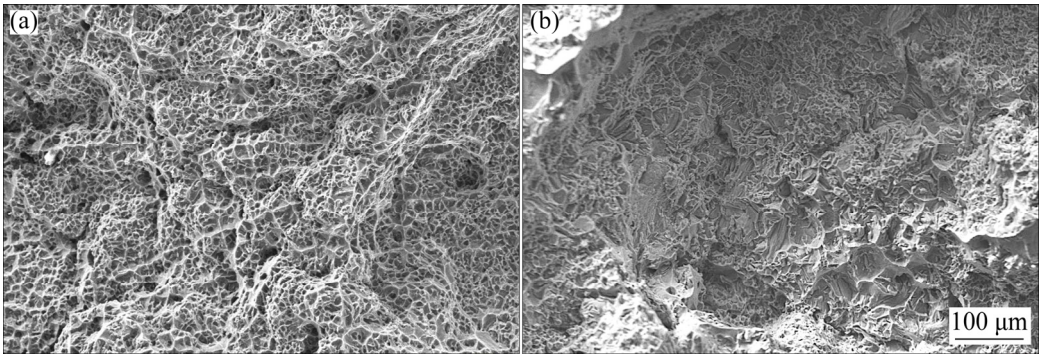

Fig. 12 SEM images showing fracture surfaces of FS (a) and CS (b) T6-RT tensile samples (CS samples present larger dimples and wider interdendritic crack path compared with FS samples)

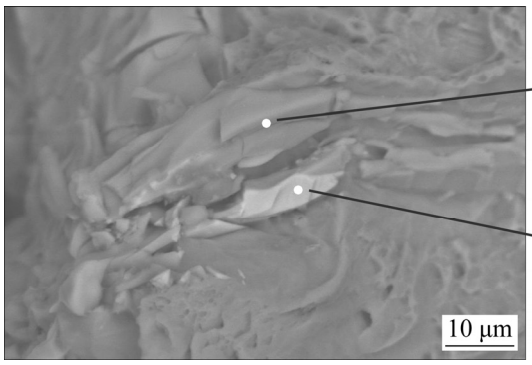

Element	wt.%	at.%
O	2.38	4.19
Mg	31.60	36.71
Al	18.23	19.07
Si	33.49	33.67
Cu	14.31	6.36

Element	wt.%	at.%
O	6.03	12.90
Mg	0.51	0.72
Al	48.16	61.06
Si	1.34	1.63
Cu	43.39	23.36

Fig. 13 SEM image and EDS analyses of cracked Cu-based intermetallic particles on fracture surface of CS T6-RT tensile sample (YS=327 MPa, UTS=359 MPa, Elongation=2.4%)

observation confirms the findings of previous works by PANG et al [29] on the detrimental role played by the oxides on the fatigue strength of aluminium castings and points out that the Fe-rich phases developed in the A357−Cu alloy can act as crack nucleation site only in synergy with other casting defects and, therefore, are less detrimental to fatigue strength than the Fe-rich phases present in the C355 alloy, such as acicular β-Al_5FeSi or large blocky π-Fe ($Al_8Mg_3FeSi_6$) as also observed by CESCHINI et al [10].

In a few cases, small pores close to the surface were identified as nucleation sites (Fig. 14), confirming that HIP is not effective on pores located close to the sample surface.

Fatigue striations are clearly identifiable in the crack propagation zones (Fig. 15), where secondary cracks are observed as well, while the overload failure region has the same ductile morphology previously described for the tensile specimen.

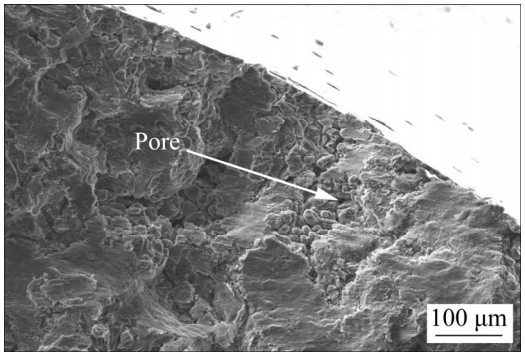

Fig. 14 SEM image of crack nucleation site in correspondence of pore in CS T6-200 °C fatigue specimen tested at 110 MPa and failed after 5.8×10^5 cycles

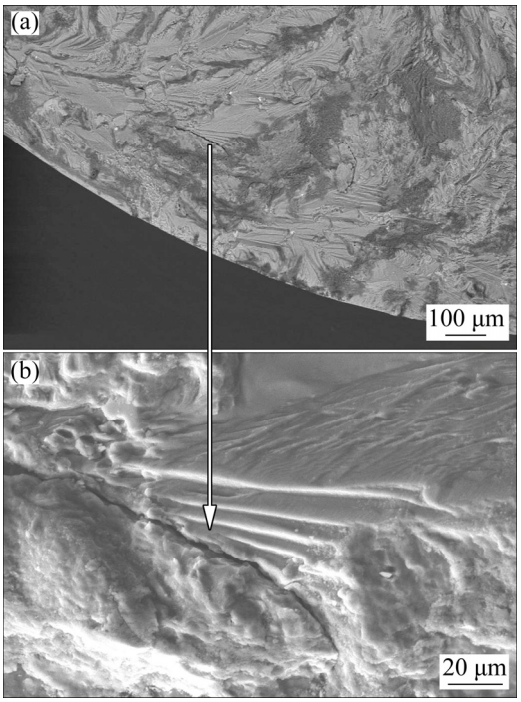

Fig. 15 SEM images of fatigue striation features and secondary cracks in FS T6-200 °C fatigue sample tested at 110 MPa and failed after 1.7×10^6 cycles

4 Conclusions

(1) A proper combination of HIP and solution treatment parameters was defined in order to avoid the incipient melting of Cu-based low melting compounds present in the A357−Cu alloy.

(2) The heat treatment was more effective on samples with fine SDAS compared to samples with coarse SDAS. This led to an improvement in the mechanical behaviour of FS samples compared to CS, mainly at room temperature.

(3) Among the studied alloys, A357−Cu alloy showed the best mechanical properties at room temperature, while at 200 °C, in the overaged

condition, both tensile and fatigue behaviour was comparable to that of the C355 alloy.

(4) After long-term exposure to high temperature, the effect of SDAS on tensile and fatigue properties of A357−Cu appeared negligibly.

(5) The fatigue resistance and the elongation to failure of the A357−Cu and C355 alloys were significantly influenced by the presence of Fe-based intermetallics and oxides.

Acknowledgments

We wish to thank Dr. Andrea Morri at Industrial Research Centre for Advanced Mechanics and Materials (CIRI-MAM) of the University of Bologna for his support to experimental work.

References

[1] JAVIDANI M, LAROUCHE D. Application of cast Al−Si alloys in internal combustion engine components [J]. International Materials Reviews, 2014, 59(3): 132−158.

[2] TAGHIABADI R, FAYEGH A, PAKBIN A, NAZARI M, GHONCHEH M H. Quality index and hot tearing susceptibility of Al−7Si−0.35Mg−*x*Cu alloys [J]. Transactions of Nonferrous Metals Society of China, 2018, 28: 1275−1286.

[3] FARKOOSH A R, PEKGULERYUZ M. Enhanced mechanical properties of an Al−Si−Cu−Mg alloy at 300 °C: Effects of Mg and the Q-precipitate phase [J]. Materials Science and Engineering A, 2015, 621: 277−286.

[4] MOHAMED A M A, SAMUEL F, KAHTANI S A. Influence of Mg and solution heat treatment on the occurrence of incipient melting in Al−Si−Cu−Mg cast alloys [J]. Materials Science and Engineering A, 2012, 543: 22−34.

[5] MOHAMED A M A, SAMUEL F, KAHTANI S A. Microstructure, tensile properties and fracture behavior of high temperature Al−Si−Mg−Cu cast alloys [J]. Materials Science and Engineering A, 2013, 577: 64−72.

[6] LASA L, RODRIGUES-IBABE J. Evolution of the main intermetallic phases in Al−Si−Cu−Mg casting alloys during solution treatment [J]. Journal of Material Science, 2004, 39: 1343−1355.

[7] HAN Y, SAMUEL A M, DOTY H W, VALTIERRA S, SAMUEL F H. Optimizing the tensile properties of Al−Si−Cu−Mg 319-type alloys: Role of solution heat treatment [J]. Materials & Design, 2014, 58: 426−438.

[8] CESCHINI L, MORRI A, MORRI A N, TOSCHI S, JOHANSSON S, SEIFEDDINE S. Effect of microstructure and overaging on the tensile behavior at room and elevated temperature of C355-T6 cast aluminum alloy [J]. Materials & Design, 2015, 83: 626−634.

[9] CESCHINI L, MORRI A, TOSCHI S, JOHANSSON S, SEIFEDDINE S. Microstructural and mechanical properties characterization of heat treated and overaged cast A354 alloy with various SDAS at room and elevated temperature [J]. Materials Science and Engineering A, 2015, 648: 340−349.

[10] CESCHINI L, MORRI A, TOSCHI S, SEIFEDDINE S. Room and high temperature fatigue behaviour of the A354 and C355 (Al−Si−Cu−Mg) alloys: Role of microstructure and heat treatment [J]. Materials Science and Engineering A, 2016, 653: 129−138.

[11] SEIFEDDINE S. Characteristics of cast aluminium–silicon alloys: Microstructures and mechanical properties [D]. Linköping, Sweden: Linköping Studies in Science and Technology, 2006.

[12] ASTM E10-18. Standard test method for Brinell hardness of metallic materials [S]. West Conshohocken, PA: ASTM International, 2018, www.astm.org.

[13] ISO 6892–1. Metallic materials – tensile testing – Part 1: Method of test at room temperature [S]. 2016.

[14] ISO 6892–2. Metallic materials – tensile testing – Part 2: Method of test at elevated temperature [S]. 2016.

[15] UNI3964–85. Mechanical testing of metallic materials fatigue testing at room temperature [S]. 1985.

[16] CESCHINI L, MORRI A, MORRI A N, PIVETTI G. Predictive equations of the tensile properties based on alloy hardness and microstructure for an A356 gravity die cast cylinder head [J]. Materials & Design, 2011, 32: 1367−1375.

[17] WANG Gui-qing, BIAN Xiu-fang, WANG Wei-min, ZHANG Jun-yan. Influence of Cu and minor elements on solution treatment of Al−Si−Cu−Mg cast alloys [J]. Materials Letters, 2003, 57(24−25): 4083−4087.

[18] ZAMANI M, TOSCHI S, MORRI A, CESCHINI L, SEIFEDDINE S. Effect of Mo addition on room and high temperature tensile behavior of Al−Si−Cu−Mg alloy in as-cast and heat-treated conditions [J]. Advanced Materials Research, 2019, 1155: 71−79.

[19] SAMUEL F. Incipient melting of Al5Mg8Si6Cu2 and Al_2Cu intermetallics in unmodified and strontium-modified Al−Si−Cu−Mg (319) alloys during solution heat treatment [J]. Journal of Material Science, 1998, 33: 2283−2297.

[20] SJÖLANDER E, SEIFEDDINE S. Optimization of solution treatment of cast Al−7Si−0.3Mg and Al−8Si−3Cu−0.5Mg alloys [J]. Metallurgical and Materials Transactions A, 2014, 45: 1916−1927.

[21] ZAMANI M, TOSCHI S, MORRI A, CESCHINI S, SEIFEDDINE S. Optimisation of heat treatment of Al−Cu−(Mg−Ag) cast alloys [J]. Journal of Thermal Analysis and Calorimetry, 2020, 139(6): 3427−3440.

[22] ZAMANI M, SEIFEDDINE S, JARFORS A E W. High temperature tensile deformation behavior and failure mechanisms of an Al−Si−Cu−Mg cast alloy — The microstructural scale effect [J]. Materials & Design, 2015, 86: 361−370.

[23] TIRYAKIOĞLU M, CAMPBELL J, STALEY J T. The influence of structural integrity on the tensile deformation of cast Al−7wt.%Si−0.6wt.%Mg alloys [J]. Scripta Materialia, 2003, 49: 873−878.

[24] WANG Qui-gui. Microstructural effects on the tensile and fracture behaviour of aluminum casting alloys A356/357 [J]. Met Mater Trans A, 2003, 34: 2887−2899.

[25] CESCHINI L, MORRI A, MORRI A N, GAMBERINI A, MESSIERI S. Correlation between ultimate tensile strength and solidification microstructure for the sand cast A357 aluminium alloy [J]. Materials & Design, 2009, 30: 4525−4531.

[26] TÓTH L, YAREMA S Y. Formation of the science of fatigue of metals (Part 1) [J]. Materials Science, 2006, 42: 87−94.

[27] LI Zhen-ming, WANG Qui-gui, LUO A A, FU Peng-huai,

PENG Li-ming. Fatigue strength dependence on the ultimate tensile strength and hardness in magnesium alloys [J]. International Journal of Fatigue, 2015, 80: 468−476.
[28] PANG Jian-chao, LI Shou-xin, WANG Zhong-guang, ZHANG Zhe-feng. General relation between tensile strength and fatigue strength of metallic materials [J]. Materials Science and Engineering A, 2013, 564: 331−341.
[29] PANG Jian-chao, LI Shou-xin, WANG Zhong-guang, ZHANG Zhe-feng. Relations between fatigue strength and other mechanical properties of metallic materials [J]. Fatigue & Fracture of Engineering Materials & Structures, 2014, 37: 958−976.
[30] BANNANTINE J A, COMER J J, HANDROCK J L, Fundamentals of metal fatigue analysis [M]. New Jersey: Prentice Hall – Englewood Cliffs, 1990.
[31] CESCHINI L, BOROMEI I, MORRI A. SEIFEDDINE S, SVENSSON I L. Microstructure, tensile and fatigue properties of the Al−10%Si−2%Cu alloy with different Fe and Mn content cast under controlled conditions [J]. Journal of Materials Processing Technology, 2009, 209: 5669−5679.
[32] WANG Qui-gui, APELIAN D, LADOS D A. Fatigue behaviour of A356-T6 aluminum cast alloys (Part I): Effect of casting defects [J]. Journal of Light Metals, 2001, 1: 73−84.
[33] WANG Qui-gui, APELIAN D, LADOS D A. Fatigue behaviour of A356/357 aluminum cast alloys (Part II): Effect of microstructural constituents [J]. Journal of Light Metals, 2001, 1: 85−97.
[34] LATTANZI L, FABRIZI A, FORTINI A, MERLIN M, TIMELLI G. Effects of microstructure and casting defects on the fatigue behavior of the high-pressure die-cast AlSi9Cu3(Fe) alloy [J]. Procedia Structural Integrity, 2017, 7: 505−512.
[35] ZHENG Yan, XIAO Wen-long, GE Su-jing, ZHAO Wei-tao, HANADA S, MA Chao-li. Effects of Cu content and Cu/Mg ratio on the microstructure and mechanical properties of Al−Si−Cu−Mg alloys [J]. Journal of Alloys and Compounds, 2015, 649: 291−296.
[36] BALDUCCI E, CESCHINI L, MESSIERI S, HOLMESTAD R, WENNER S. Thermal stability of the lightweight 2099 Al−Cu−Li alloy: Tensile tests and microstructural investigations after overaging [J]. Materials and Design, 2017, 119: 54−64.
[37] DI GIOVANNI M T, MØRTSELL E A, SAITO T, AKHTAR S, DI SABATINO M, LI Y, CERRI E. Influence of Cu addition on the heat treatment response of A356 foundry alloy [J]. Materials Today Communications, 2019, 19: 342−348.
[38] CACERES C H, DAVIDSON C, GRIFFITHS J. The deformation and fracture behavior of an Al−Si−Mg casting alloy [J]. Materials Science and Engineering A, 1995, 197: 171−179.
[39] PENG Ji-hua, TANG Xiao-long, HE Jian-ting, XU De-ying. Effect of heat treatment on microstructure and tensile properties of A356 alloys [J]. Transactions of Nonferrous Metals Society of China, 2011, 21: 1950−1956.

添加 Cu 对 A357 合金过时效行为及室温、高温拉伸和疲劳性能的影响

Lorella CESCHINI[1], Simone MESSIERI[2], Alessandro MORRI[1],
Salem SEIFEDDINE[3], Stefania TOSCHI[4], Mohammadreza ZAMANI[3]

1. Department of Industrial Engineering (DIN), Alma Mater Studiorum, University of Bologna, Viale Risorgimento 4, 40136 Bologna, Italy;
2. Ducati Motor Holding, Via Cavalieri Ducati Antonio 3, 40132 Bologna, Italy;
3. Department of Materials and Manufacturing, School of Engineering, Jönköping University, Gjuterigatan 5, 55111 Jönköping, Sweden;
4. Department of Civil, Chemical, Environmental and Materials Engineering (DICAM), Alma Mater Studiorum, University of Bologna, Viale Risorgimento 4, Bologna, Italy

摘　要：本研究的目的是通过研究富铜合金在室温和 200 °C 下的抗拉强度和疲劳强度以评估合金的过时效行为，并将力学性能与其显微组织，尤其是二次枝晶臂间距(SDAS)相关联。在 200 °C 下对过时效合金进行力学性能测试，结果显示，在 A357 合金中添加 1.3%(质量分数)Cu 能够使其极限抗拉强度、屈服强度和疲劳强度分别保持在近 210、200 和 100 MPa。与四元(Al−Si−Cu−Mg)C355 合金相比，A357−Cu 合金具有更高的室温力学性能和相当的高温(200 °C)力学性能。显微组织分析表明，SDAS 对峰值时效 A357−Cu 合金的室温力学行为有影响，而对过时效合金在 200 °C 的拉伸和疲劳性能影响甚微。

关键词：A357 合金；C355 合金；Al−Si−Cu−Mg 铸造合金；拉伸性能；疲劳行为；高温；过时效

(Edited by Xiang-qun LI)